Journal of The Electrochemical Society, **158** (10) H994-H996 (2011)
0013-4651/2011/158(10)/H994/3/$28.00 © The Electrochemical Society

Defect Reduction in Semipolar (11-22) GaN Grown on m-Sapphire Using Epitaxial Lateral Overgrowth

Sung-Nam Lee,[a,z,*] Jihoon Kim,[a,b] and Hyunsoo Kim[c,*]

[a]*Department of Nano-Optical Engineering, Korea Polytechnic University, Siheung 429-793, Korea*
[b]*Future Convergence Ceramic Division, Korea Institute of Ceramic Engineering and Technology, Seoul 153-801, Korea*
[c]*School of Semiconductor and Chemical Engineering and Semiconductor Physics Research Center, Chonbuk National University, Jeonju 561-756, Korea*

We investigated the optical and the crystal qualities of epitaxial lateral overgrown (ELO) semipolar (11-22) GaN produced using three growth steps: growth of the seed layer for the [11-20] a-direction, the formation of a semipolar (11-22) plane, and the lateral coalescence step with a [11-22] direction. Fully-coalesced ELO-GaN had a good surface morphology and a very low defect density of $\sim 5.5 \times 10^5$ cm^{-2}, which was smaller than that of conventional c-plane ELO-GaN. In spite of the generation of some crystallographic tilts, the crystal properties were significantly enhanced as a result of the ELO process. The cathodeluminescence intensity of band edge emission in the low defect region was about 3.1 times higher than in the highly defective region, indicating that the optical properties of semipolar GaN could be significantly enhanced by reducing defects.
 [DOI: 10.1149/1.3617468]

Manuscript submitted May 6, 2011; revised manuscript received June 27, 2011. Published August 2, 2011.

Recently, remarkable progress on the development of high efficiency GaN-based optoelectronic devices has been achieved by some research groups, which reported the development of commercial grade GaN-based laser diodes (LDs) and visible light emitting diodes (LEDs).[1–3] However, it is well known that the wurzite GaN-based light emitting devices grown along the [0001] c-axis suffer from a reduced radiative efficiency and a redshift of the optical transition due to spontaneous and strain-induced polarization.[4–7] These problems can be overcome by using the nonpolar a-plane or m-plane GaN epilayer.[8–12] However, there are some growth issues to achieve a high quality nonpolar GaN epilayer. Alternatively, the electric field can also be reduced by using a semipolar GaN film. Thereby, the quantum confined stark effect (QCSE) in a strained semipolar (11-22) InGaN layer has been calculated to be 80% lower than that on the polar c-plane.[8] The semipolar GaN has the additional advantage of higher In incorporation rate in the semipolar plane, which gives the possibility for enhanced radiative efficiency in the green gap region.[13]

In the heteroepitaxial growth of semipolar GaN epilayers, the defect density of semipolar GaN films is much higher than that of conventional c-plane GaN epilayers. It has been reported that threading dislocations (TDs) of $\sim 10^{10}$/cm^2 and basal stacking faults (BSFs) of $\sim 10^5$/cm^2 in semipolar (11-22) GaN on m-plane sapphire[14–19] result in the limitation of internal quantum efficiency of the semipolar InGaN active layer.[20,21] Recently, the best performance of semipolar GaN-based LED/LDs has been achieved by using a high quality semipolar GaN substrate with much lower TDs and BSFs.[22,23] However, high quality semipolar GaN substrate has the disadvantages of very high price and small size. To commercialize high efficiency semipolar GaN-based LED/LDs, the defect density of heteroepitaxial semipolar GaN epilayer must be reduced to the level of the semipolar GaN substrate. Among the defect reduction methods, epitaxial lateral overgrowth (ELO) is a widely used defect reduction technique for III-nitride systems.[14–19] However, it is very difficult to obtain high quality fully-coalesced semipolar ELO-GaN with good surface morphology due to the anisotropic crystallographic properties. In this study, we report the results of fully-coalesced semipolar ELO-GaN with a very low defect density by using a three-step growth technique.

Until now, most research groups have focused on the growth mode and dislocation behavior rather than the surface morphology of semipolar ELO-GaN (Refs. 15–19) because of severe difficulties in planarization and coalescence of the lateral growth step. However, one can see that, in spite of the existence of some waves in the surface as shown in Fig. 2a, there is good surface morphology without any pits or non-coalesced surface structures after three-step growth. This is confirmed in Figs. 2a and 2b, which were observed using a Nomarski optical microscope (NOM) and an atomic force microscope (AFM), respectively. From AFM measurements, surface RMS roughness of semipolar ELO-GaN was 17.3 nm which was relatively rougher surface than that of conventional semipolar GaN. However, we believed that surface morphology would be enhanced by optimization of growth conditions.

From high resolution X-ray diffraction (HR-XRD), we investigated the crystal qualities of semipolar GaN and ELO-GaN on m-sapphire with different two incident beam directions of [1-100] and [11-2-3]. Further, to understand the dependence of crystal qualities of the semipolar ELO-GaN template on each ELO-step, we performed an X-ray ω-rocking scan for $\Phi = 0°$ (solid line) and $\Phi = 90°$ (broken like), where the azimuth is the angle between the stripe direction and the rotation axis of the ω scan. Figure 3a shows ω-rocking curves of as-grown (11-22) semipolar GaN/m-sapphire, whose full width at half maximums (FWHMs) were near 620 and 1165 arcsec for $\Phi = 0$ and 90°, respectively. Before full coalescence (Step II), FWHMs were significantly decreased to near 420 and 291 arcsec for $\Phi = 0$ and 90°, respectively, as shown in Fig. 3b. This can be ascribed to the reduction in defect density during epitaxial lateral growth. After full coalescence (Step III), it is found that FWHMs for $\Phi = 90°$ were further reduced to 260 arcsec, whereas that for $\Phi = 0°$ was drastically increased to 740 arcsec. Moreover, three peaks were found in the XRD curve for $\Phi = 0°$, resulting in a broad FWHM, as shown in Fig. 2c. This implied that the significant difference of FWHMs between $\Phi = 0°$ and $\Phi = 90°$ is caused by the generation of crystallographic tilt during the coalescence step.

The optical properties of semipolar ELO-GaN templates were characterized by room temperature cathode luminescence (CL) analysis using a Hitachi S-4700 system installed on a field-emission scanning electron microscope. Figure 4a showed the panchromatic CL image of semipolar (11-22) ELO-GaN on m-sapphire at the emission peak with a wavelength of 362 nm, known by the near band edge emission of GaN. In Fig. 4a, one can see that there are wide bright regions and dark spot regions, representing low defect regions and high defect regions, respectively. Regarding the dislocation density of ELO-GaN, we can clearly find a very low dislocation density of 5.5×10^5 cm^{-2}, measured from the dark spot density in lateral growth regions. Compared with the defect density ($1.0–5.0 \times 10^6$ cm^{-2}) of conventional c-plane ELO-GaN templates and the freestanding GaN substrate, the defect density of our semipolar ELO-GaN template is low enough to enhance the performance of light emitting devices.

In addition, we measured CL spectra for two different positions which were the bright point (position A) in the low defect zone and the dark point (position B) in the high defect zone, as shown in Fig. 4b. The CL intensity of position A is about 3.1 times higher

* Electrochemical Society Active Member.
z E-mail: snlee@kpu.ac.kr

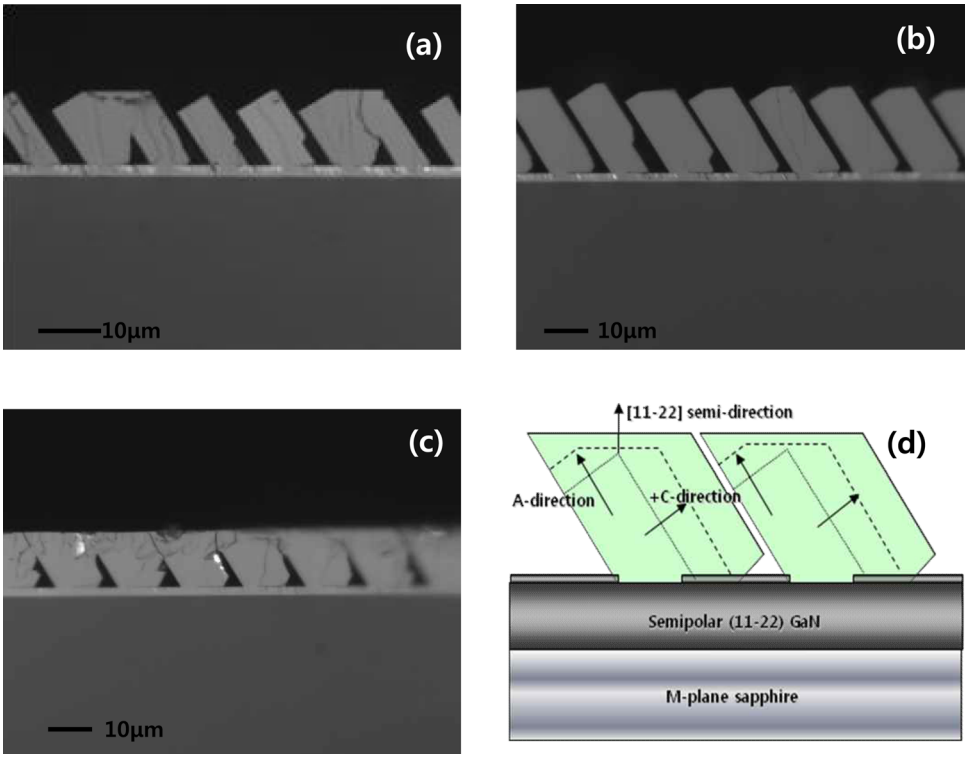

Figure 1. (Color online) Optical microscopy cross-section images of semipolar ELO-GaN for three-step growth: (a) seed layer growth for a-direction (Step I), (b) the formation of a semipolar plane (Step II), and (c) lateral growth in the c-direction (Step III). (d) Schematic growth procedures of semipolar ELO-GaN with three steps.

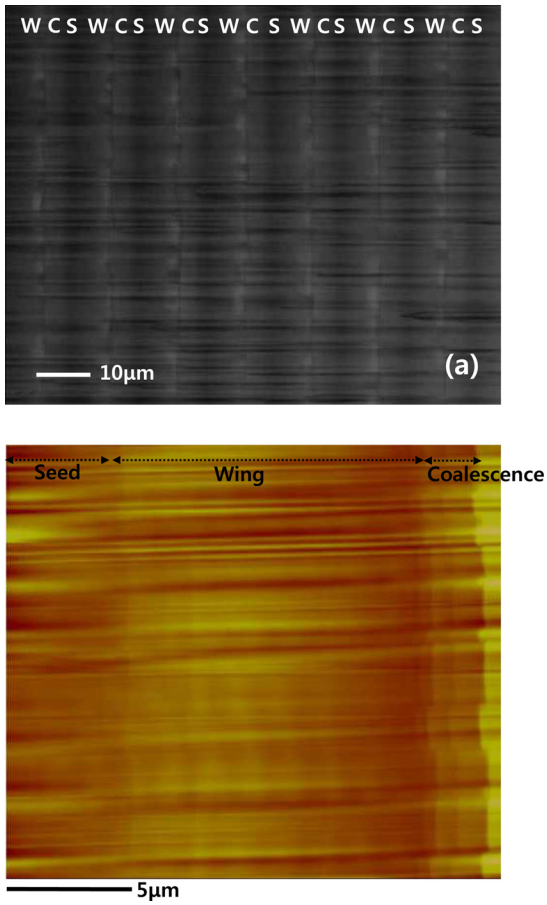

Figure 2. (Color online) The surface images of the fully-coalesced semipolar (11-22) ELO-GaN measured by (a) Normalski optical microscope and (b) atomic force microscope (20 μm $\times$ 20 μm). (*W: wing region, C: coalescence region, and S: seed GaN layer*).

than that of position B. This indicates that the optical properties of semipolar GaN were significantly affected by dislocation density because a dislocation may act as a non-radiative recombination center in GaN epilayers.[14] The emission energy of band edge at position A (3.427 eV) was slight higher than position B (3.420 eV). Since the broad band at 3.41 eV corresponds to a BSFs-related peak,[17] this

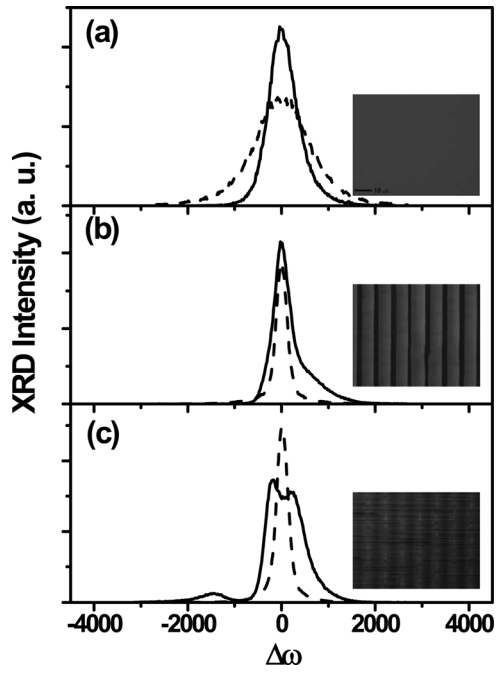

Figure 3. X-ray ω-rocking scan of (a) as-grown semipolar GaN/m-sapphire, (b) partially coalesced ELO-GaN, and (c) fully-coalesced ELO-GaN template for $\Phi = 0°$ (solid line) and $\Phi = 90°$ (broken like), where the azimuth is the angle between the stripe direction and the rotation axis of the ω scan. Insets are optical microscope images of ELO-GaN for each step.

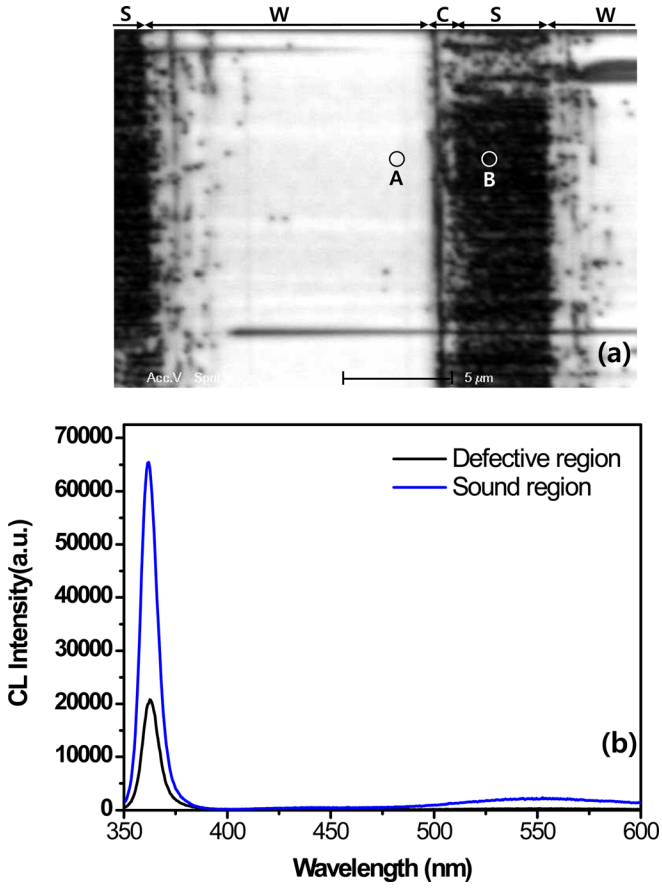

Figure 4. (Color online) (a) The panchromatic CL image of semipolar (11-22) ELO-GaN on sapphire at the emission peak with wavelengths of 362 nm and (b) CL spectra for two different positions which were the bright point (position A) in the low defect region and the dark point (position B) in the high defect region. (*W: wing region, C: coalescence region, and S: seed GaN layer*).

relative low emission energy can be ascribed to remaining TDs and BSFs in the defective region.

In conclusion, we obtained fully-coalesced semipolar (11-22) ELO-GaN/m-plane sapphire by using three-step growth. In spite of some wavy surface structures, there is relative good surface morphology without any pits or non-coalesced regions in the whole wafer. However, for fully-coalesced ELO-GaN, the significant difference of XRC FWHMs between $\Phi = 0^\circ$ and $\Phi = 90^\circ$ is likely caused by the generation of crystallographic tilt in the direction of lateral growth during the coalescence step. In the lateral growth region, the defect density of ELO-GaN was 5.5×10^5 cm^{-2}, which is smaller than that of the conventional c-plane ELO-GaN or free-standing GaN. These results imply that semipolar ELO-GaN will be applied to enhance the high efficiency of light emitting devices.

This research was supported by the IT R&D program of MKE/KEIT [10039151, The development of 200 mW level high power green (525 nm) LED for full color display] and Core Corporation Research Program (2010-0026523) through the National Research Foundation of Korea (NRF) funded by the Ministry of Education, Science and Technology.

References

1. M. Geneghini, N. Trivellin, M. Manfredi, U. Zehnder, B. Hahn, G. Meneghesso, and E. Zanoni, *Appl. Phys. Lett.*, **95**, 173507 (2009).
2. M. F. Schubert, J. Xu, J. K. Kim, E. F. Schubert, M. H. Kim, S. Yoon, S. M. Lee, C. Sone, T. Sakong, and Y. Park, *Appl. Phys. Lett.*, **93**, 041102 (2008).
3. A. Avramescu, T. Lermer, J. Muller, S. Tautz, D. Queren, S. Lutgen, and U. Strauβ, *Appl. Phys. Lett.*, **95**, 071103 (2009).
4. P. Waltereit, O. Brandt, A. Trampert, H. T. Grahn, J. Menniger, M. Ramsteiner, M. Reiche, and K. H. Ploog, *Nature*, **406**, 865 (2000).
5. S. F. Chichibu, A. C. Abare, M. S. Minsky, S. Keller, S. B. Fleischer, J. E. Bowers, E. Hu, U. K. Mishra, L. A. Coldren, S. P. DenBaars, and T. Sota, *Appl. Phys. Lett.*, **73**, 2006 (1998).
6. U. T. Schwarz, H. Braun, K. Kojima, Y. Kawakami, S. Nagahama, and T. Mukai, *Appl. Phys. Lett.*, **91**, 123503 (2007).
7. S. N. Lee, H. Y. Ryu, H. S. Paek, J. K. Son, Y. J. Sung, K. S. Kim, H. K. Kim, H. Kim, T. Jang, K. H. Ha, O. H. Nam, and Y. Park, *IEEE Electron Device Lett.*, **29**, 870 (2008).
8. U. Schwarz and M. Kneissl, *Phys. Status Solidi (RRL)*, **1**, A44 (2007).
9. S. N. Lee, H. S. Paek, J. K. Son, T. Sakong, O. H. Nam, and Y. Park, *J. Cryst. Growth*, **307**, 358 (2007).
10. M. D. Craven, P. Waltereit, J. S. Speck, and S. P. DenBaars, *Appl. Phys. Lett.*, **84**, 496 (2004).
11. A. Chakraborty, B. A. Haskell, S. Keller, J. S. Speck, S. P. DenBaars, S. Nakamura, and U. K. Mishira, *Jpn. J. Appl. Phys.*, **44**, L173 (2005).
12. X. Ni, M. Wu, J. Lee, X. Li, A. A. Baski, U. Ozgur, and H. Morkoc, *Appl. Phys. Lett.*, **95**, 111102 (2009).
13. Y. Kawakami, K. Nishizuka, D. Yamada, A. Kaneta, M. Funato, Y. Narukawa, and T. Mukai, *Appl. Phys. Lett.*, **90**, 261912 (2007).
14. S. N. Lee, H. S. Paek, H. Kim, Y. M. Park, T. Jang, and Y. Park, *Appl. Phys. Lett.*, **92**, 111106 (2008).
15. X. Ni, U. Ozgur, A. A. Baski, H. Morkoc, L. Zhou, D. J. Smith, and C. A. Tran, *Appl. Phys. Lett.*, **90**, 182109 (2007).
16. P. de Mierry, N. Kriouche, M. Nemoz, and G. Nataf, *Appl. Phys. Lett.*, **94**, 191903 (2009).
17. T. Guhne, Z. Bougrioua, P. Vennegues, M. Leroux, and M. Albrecht, *J. Appl. Phys.*, **101**, 113101 (2007).
18. P. Vennegues, Z. Bougrioua, and T. Guehne, *Jpn. J. Appl. Phys.*, **46**, 4089 (2007).
19. N. Kriouche, M. Lerous, P. Vennegues, M. Nemoz, G. Nataf, and P. deMierry, *Nanoscale Res. Lett.*, **5**, 1878 (2010).
20. M. Funato, M. Ueda, Y. Kawakami, Y. Narukawa, T. Kosugi, M. Takahashi, and T. Mukai, *Jpn. J. Appl. Phys.*, **45**, L659 (2006).
21. B. Neubert, T. Wunderer, P. Bruckner, F. Scholz, M. Feneberg, F. Lipski, M. Schirra, and K. Thonke, *J. Cryst. Growth*, **298**, 706 (2007).
22. H. Sato, A. Tyagi, H. Zhong, N. Fellows, R. Chung, M. Saito, K. Fujito, J. S. Speck, S. P. DenBaars, and S. Nakamura, *Phys. Status. Solidi (RRL)*, **1**, 162 (2007).
23. Y. Enya, Y. Yoshizumi, T. Kyono, K. Akita, M. Ueno, M. Adachi, T. Sumitomo, S. Tokuyama, T. lkegami, K. Katayama, and T. Nakamura, *Appl. Phys. Express*, **2**, 082101 (2009).
24. S. N. Lee, K. K. Kim, J. H. Kim, O. H. Nam, and H. Kim, *Phys. Status Solidi C*, **7**, 2043 (2010).